

IgA-BEM for 3D Helmholtz problems on multi-patch domains using B-spline tailored numerical integration

Antonella Falini^a, Tadej Kanduč^{*b,c}, Maria Lucia Sampoli^d, Alessandra Sestini^e

^a*Dipartimento di Informatica, Università degli Studi di Bari Aldo Moro,
Via Orabona 4, Bari, Italy*

^b*Faculty of Mathematics and Physics, University of Ljubljana,
Jadranska ulica 19, 1000 Ljubljana, Slovenia*

^c*Faculty of Mechanical Engineering, University of Ljubljana,
Aškerčeva cesta 6, 1000 Ljubljana, Slovenia*

^d*Department of Information Engineering and Mathematics, University of Siena,
Via Roma 56, Siena, Italy*

^e*Department of Mathematics and Computer Science, University of Firenze,
Viale Morgagni 67, Firenze, Italy*

Abstract

An Isogeometric Boundary Element Method (IgA-BEM) is considered for the numerical solution of Helmholtz problems on 3D domains admitting a smooth conformal multi-patch representation of the boundary surface. The discretization space is formed by C^0 inter-patch continuous basis functions whose restriction to a patch simplifies to the span of tensor product B-splines composed with the given patch parameterization. To profit by efficient function-by-function matrix assembly, the proposed model utilizes a spline quasi-interpolation numerical integration procedure for both singular and regular integrals defined on the support of each B-spline basis function in the discretization space. In particular, in the singular case the scheme combines a singularity extraction technique with a B-spline recursion. Numerical examples on relevant benchmarks show that the expected convergence orders are achieved with a small number of quadrature nodes.

Keywords: Helmholtz equation, Isogeometric Analysis (IgA), Boundary Element Method (BEM), singular integrals, quadrature formulas, B-splines, quasi-interpolation, assembly

1. Introduction

Isogeometric analysis (IgA) [7] is a powerful approach for the numerical solution of problems governed by partial differential equations, introduced in the literature at the beginning of the new millennium. This new paradigm was motivated by the observation that in engineering applications a domain is described by its boundary parametric representation generated by Computer Aided Design (CAD) software. For this aim CAD relies on flexible forms, often based on multi-patch tensor product B-spline or rational B-spline (NURBS) spaces, suited also for applications [13]. Actually the IgA idea consists in adopting the CAD functional spaces also for approximating the solution of the differential problems, taking into account the well-known optimal approximation power of spline spaces [8, 20]. The increasing success of the IgA paradigm in the context of both domain and boundary element methods is easily explained considering that, besides being capable to keep an exact representation of complex domains described in a multi-patch CAD form, IgA formulations guarantee a certain level of accuracy with considerably less degrees of freedom than traditional Finite Element Analysis (FEA), which relies on larger piecewise polynomial spaces with lower inter-element smoothness within each patch. The attractiveness of IgA is even higher focusing on boundary element methods (BEMs), see for example [22, 1, 3] and references therein, because, in contrast to domain methods like

*Corresponding Author

Email address: tadej.kanduc@fmf.uni-lj.si (Tadej Kanduč*)

FEM, they do not require any preliminary volumetric parameterization, which can be a remarkably time consuming task. BEMs rely on a boundary integral formulation of the problem, which can be derived whenever the fundamental solution of the associated differential operator is known. Hence, they require only the definition of a mesh on the boundary of the domain, which is a much easier task especially in the IgA context, where the CAD representation of the boundary is available.

The precursor of this work, dealing with 3D IgA-BEM, is presented in [10], where exterior Laplace problems with Dirichlet boundary conditions on single patch domains are considered and, in order to deal also with screen problems, an indirect boundary integral formulation is adopted. In this paper the IgA multi-patch formulation of BEMs (multi-patch IgA-BEMs) based on a direct boundary integral formulation is considered for the numerical solution of problems governed by the Helmholtz equation on 3D bounded or even unbounded domains, equipped with either Dirichlet or Neumann boundary conditions. Such problems are of interest in acoustics, since they model radiation and rigid scattering in the frequency domain [16], where radiation refers to the pressure field produced by an object vibrating within a fluid (usually air or water), while rigid scattering relates to the disturbance caused by an obstacle immersed within an existing acoustic field. The adopted boundary integral equation (BIE) discretized with a collocation approach is the so-called conventional BIE (CBIE), which involves only weakly singular integrals and is augmented with the Sommerfeld radiation condition at infinity for exterior problems. The Helmholtz operator can thus be simply written as a sum of the Laplacian Δ with an identity operator scaled with a positive parameter κ^2 . However, even when dealing with exterior Helmholtz problems admitting a unique solution, such BIE generates spurious solutions when κ^2 is an eigenvalue of $-\Delta$ for the considered boundary conditions. This is the reason why other papers also relying on IgA-BEMs for the numerical solution of the Helmholtz equation introduce its alternative Burton-Miller (BM) boundary integral formulation, which does not suffer from such drawback. Obtained as a linear combination of the mentioned CBIE with the hypersingular BIE (HBIE) also paired with the Helmholtz operator, the BM integral formulation is clearly more difficult, see for example [23], where it is combined with a regularization technique to avoid to deal with hypersingular integrals in the assembly phase. However, successive researches have given numerical evidence that, when κ^2 is not an eigenvalue of $-\Delta$, better numerical results are achieved by using the simpler CBIE, see for example [25, 21]. Since clearly only a finite number of different values of the parameter κ^2 can be considered and this can be anyway sufficient for a reasonable reconstruction of an associated time-dependent acoustic field, we have opted for applying the IgA-BEM approach just to the CBIE associated with Helmholtz, with the implicit assumption to avoid values of κ^2 equal to eigenvalues of $-\Delta$.

The IgA-BEM implementation in this study relies on the B-spline tailored cubature formulas for regular and weakly singular integrals, firstly introduced in [12] for surface weakly singular integrals and generalized in [15] to achieve better approximation properties for general smooth geometry parametrizations. The rules incorporate a singularity subtraction step for singular integrals, which is capable to control the continuity of the obtained regularized integrands. The cubature rules descend from the Hermite spline Quasi-Interpolation (QI) approach introduced in [17] and generalized to the tensor product setting. In particular, in order to require only function values at integration nodes, a derivative free approach, firstly studied in univariate case in [18], is implemented. The extension to the tensor product setting of the product formula for B-splines in [19] contributes to the definition of the final rule, which ensures a seamlessly incorporation of the trial B-spline factor in the integrand. This ensures the possibility to apply the integration procedure directly on the whole support of the B-spline and consequently a fast function-by-function implementation in the matrix assembly phase. By distributing quadrature nodes uniformly, the presented procedure allows us to integrate regular and singular integrals with sufficient accuracy and with a small number of quadrature nodes.

The paper is organized as follows. The next section introduces the Helmholtz problem and its conventional boundary integral formulation for both Dirichlet and Neumann boundary conditions. Then in Section 3 the multi-patch IgA setting is presented describing the standard CAD representation of a bounded or unbounded domain, as well as the finite dimensional functional spaces adopted for the analysis. Section 4 describes the developed quadrature formulas, which are based on the tensor-product formulation of a discrete spline quasi-interpolation approach. These formulas are combined here for the first time with a subtraction (possibly high order) regularization technique and applied to the single and double layer Helmholtz kernels. Finally, in Section 5 the results obtained for some benchmark problems are reported and commented, while some conclusive remarks are given in Section 6.

2. The Helmholtz problem and its boundary integral formulation

We study 3D potential problems described by the Helmholtz equation with Dirichlet or Neumann boundary conditions on domains $\Omega^{[\ell]} \subset \mathbb{R}^3$ admitting a connected closed boundary surface $\Gamma = \partial\Omega^{[\ell]}$,

$$\begin{cases} \Delta u + \kappa^2 u = 0 & \text{in } \Omega^{[\ell]}, \\ u = u_D \quad \text{or} \quad \frac{\partial u}{\partial \mathbf{n}} = u_N & \text{on } \Gamma, \end{cases} \quad (1)$$

where $u : \Omega \rightarrow \mathbb{C}$ denotes the unknown *potential*, \mathbf{n} the unit normal on Γ pointing outward from $\Omega^{[\ell]}$ and $\kappa > 0$. When the domain is a finite volume the problem is *interior* with using the notation $\ell = i$. In the opposite case, it is set $\ell = e$ and we study the *exterior* problem. Concerning the regularity of the boundary surface Γ , for simplicity we assume to be smooth, at least without self-intersections and with a tangent plane well defined at each point and varying continuously. Note that for exterior problems, equation (1) has to be augmented with an additional condition, the so called *Sommerfeld radiation condition*,

$$\frac{\partial u}{\partial r} - i\kappa u = o\left(\frac{1}{r}\right), \quad (2)$$

where r denotes the point distance from the origin of the reference system and i is the imaginary unit; see for example [16]. This condition at infinity is necessary to ensure for any positive κ the existence and uniqueness of the solution u for exterior Helmholtz problems for both Dirichlet and Neumann boundary conditions. On this concern we observe also that, when interior problems are dealt with, uniqueness is ensured only if κ^2 is not an *eigenvalue* of the reversed Laplacian operator $-\Delta$ in Ω ¹. Regarding the regularity of the weak solution u of (1), we observe that u belongs to the Sobolev space $H^1(\Omega)$, provided that, for Dirichlet (Neumann) boundary conditions, $u_D \in H^{1/2}(\Gamma)$, ($u_N \in H^{-1/2}(\Gamma)$). The Helmholtz equation is of particular interest in acoustic because the solution $u = u(\mathbf{x}, \kappa)$, $\mathbf{x} \in \Omega$ of (1) can be interpreted as the inverse Fourier transform [24] of the time-dependent scattered pressure field $p = p(\mathbf{x}, t)$ generated by the scatterer in a given fluid domain, which fulfills the wave equation,

$$\frac{1}{c_f^2} \frac{\partial^2 p}{\partial t^2} = \Delta p. \quad (3)$$

Actually, setting

$$\check{p} = \check{p}(\mathbf{x}, \omega) := \int_{-\infty}^{+\infty} p(\mathbf{x}, t) e^{i\omega t} dt$$

it is easy to verify that \check{p} verifies the Helmholtz equation with $\kappa = \omega/c_f$ and that, conversely, it is

$$p = \frac{1}{2\pi} \int_{-\infty}^{+\infty} \check{p}(\mathbf{x}, \omega) e^{i\omega t} d\omega.$$

This is of interest because it allows to deal with a differential problem formulated just in terms of spatial variables.

In order to approximate the solution of (1) with IgA-BEMs, we consider the Conventional Boundary Integral Equation (CBIE) associated with the Helmholtz equation and derived by using a direct approach,

$$\int_{\Gamma} \mathcal{G}_{\kappa}(\mathbf{x}, \mathbf{y}) \frac{\partial u}{\partial \mathbf{n}_{\mathbf{y}}}(\mathbf{y}) d\Gamma_{\mathbf{y}} = c(\mathbf{x})u(\mathbf{x}) + \int_{\Gamma} \frac{\partial \mathcal{G}_{\kappa}}{\partial \mathbf{n}_{\mathbf{y}}}(\mathbf{x}, \mathbf{y}) u(\mathbf{y}) d\Gamma_{\mathbf{y}}, \quad \mathbf{x} \in \Gamma, \quad (4)$$

where, setting $r := \|\mathbf{r}\|_2$ with $\mathbf{r} := \mathbf{x} - \mathbf{y}$, the kernel \mathcal{G}_{κ} and its derivative with respect to the exterior unit normal \mathbf{n} to Γ are defined as follows,

$$\mathcal{G}_{\kappa}(\mathbf{x}, \mathbf{y}) := \frac{1}{4\pi r} e^{i\kappa r}, \quad \frac{\partial \mathcal{G}_{\kappa}}{\partial \mathbf{n}_{\mathbf{y}}}(\mathbf{x}, \mathbf{y}) = \frac{1}{4\pi r} e^{i\kappa r} \left(-\frac{1}{r} + i\kappa \right) \frac{\partial r}{\partial \mathbf{n}_{\mathbf{y}}},$$

¹The scalar λ is an eigenvalue for $-\Delta$ if there exists a non vanishing function u_{λ} such that $-\Delta u_{\lambda} = \lambda u_{\lambda}$, also fulfilling homogeneous boundary condition of the assigned type. It is possible to prove that the operator $-\Delta$ admits only positive eigenvalues, which define an unbounded infinite sequence of positive numbers depending on the considered kind of boundary conditions and on the shape of the finite domain Ω , see for example [14].

with

$$\frac{\partial r}{\partial \mathbf{n}_y} = -\frac{\mathbf{r} \cdot \mathbf{n}_y}{r}, \quad c(\mathbf{x}) := -\int_{\Gamma} \frac{\partial \mathcal{G}_0}{\partial \mathbf{n}_y}(\mathbf{x}, \mathbf{y}) d\Gamma_y,$$

being $c(\mathbf{x}) \equiv 1/2$ for the assumed smooth surface Γ . The restrictions of u and $(\partial u / \partial \mathbf{n})(\mathbf{y})$ to Γ are usually called *Cauchy data*, being one of them coincident with the available boundary datum and the other the unknown. By separating the real and imaginary parts of \mathcal{G}_κ , we obtain

$$\mathcal{G}_\kappa = \frac{1}{4\pi} \left(\frac{\cos(\kappa r)}{r} + i \frac{\sin(\kappa r)}{r} \right). \quad (5)$$

This expression clearly shows that we are dealing with a weakly singular kernel, since its real part goes to infinity as $1/r$ when $r \rightarrow 0^+$ (while its imaginary part tends to $\kappa/(4\pi)$). The other kernel involved in (4) is $\partial \mathcal{G}_\kappa / \partial \mathbf{n}_y$, which can be written as follows, again separating its real and imaginary parts,

$$\frac{\partial \mathcal{G}_\kappa}{\partial \mathbf{n}_y}(\mathbf{x}, \mathbf{y}) = \frac{1}{4\pi} \left[\left(\frac{\mathbf{r} \cdot \mathbf{n}_y}{r^3} (\cos(\kappa r) + \kappa r \sin(\kappa r)) \right) + i \frac{\mathbf{r} \cdot \mathbf{n}_y}{r^2} \left(\frac{\sin(\kappa r)}{r} - \kappa \cos(\kappa r) \right) \right]. \quad (6)$$

Now in the following proposition we prove that, for a regular surface Γ , the quantity $\mathbf{r} \cdot \mathbf{n}_y / r^2$ is bounded for $r \rightarrow 0^+$ but in general it is not continuous at $r = 0$. The bounded behavior at $r = 0$ of such quantity implies anyway that, analogously to \mathcal{G}_κ , the kernel $\partial \mathcal{G}_\kappa / \partial \mathbf{n}_y$ is just weakly singular, see also Section 9.1 in [2]. Actually, its real part goes to infinity as $1/r$ when $r \rightarrow 0^+$ while its imaginary part tends to zero because $\mathbf{r} \cdot \mathbf{n}_y / r^2$ remains bounded and it is multiplied by a factor going to zero.

Proposition 1. *If Γ is a regular surface admitting a C^2 parameterization, $\mathbf{X} : [a, b] \times [c, d] \rightarrow \Gamma$, for each $\mathbf{s} \in (a, b) \times (c, d)$ setting $\mathbf{t} = \mathbf{s} + \rho(\cos \theta, \sin \theta)$ it is*

$$\lim_{\rho \rightarrow 0} \frac{\mathbf{r} \cdot \mathbf{N}(\mathbf{t})}{r^2} = -\frac{1}{2} \frac{L \cos^2 \theta + 2M \sin \theta \cos \theta + N \sin^2 \theta}{E \cos^2 \theta + 2F \sin \theta \cos \theta + G \sin^2 \theta}, \quad (7)$$

where $\mathbf{r} = \mathbf{X}(\mathbf{t}) - \mathbf{X}(\mathbf{s})$, $r = \|\mathbf{r}\|_2$, $\mathbf{N}(\mathbf{t}) := \mathbf{X}_{t_1}(\mathbf{t}) \times \mathbf{X}_{t_2}(\mathbf{t})$ and E, F, G and L, M, N are respectively the coefficients of the first fundamental form ($E = \mathbf{X}_{t_1} \cdot \mathbf{X}_{t_1}$, $F = \mathbf{X}_{t_1} \cdot \mathbf{X}_{t_2}$, $G = \mathbf{X}_{t_2} \cdot \mathbf{X}_{t_2}$) of \mathbf{X} evaluated at \mathbf{s} and those of the second one times $\|\mathbf{N}(\mathbf{s})\|_2$ ($L = (\mathbf{X}_{t_1} \times \mathbf{X}_{t_2}) \cdot \mathbf{X}_{t_1, t_1}$, $M = (\mathbf{X}_{t_1} \times \mathbf{X}_{t_2}) \cdot \mathbf{X}_{t_1, t_2}$, $N = (\mathbf{X}_{t_1} \times \mathbf{X}_{t_2}) \cdot \mathbf{X}_{t_2, t_2}$).

Proof. First of all for brevity let us use the notation $\mathbf{X}_i := X_{t_i}(\mathbf{s})$ and $\mathbf{X}_{i,j} := \mathbf{X}_{t_i, t_j}(\mathbf{s})$, $i, j = 1, 2$. Then, referring to the notation introduced in the statement, we can write

$$\mathbf{X}(\mathbf{t}) - \mathbf{X}(\mathbf{s}) = \rho(\mathbf{X}_1 \cos \theta + \mathbf{X}_2 \sin \theta) + \rho^2 \left(\frac{1}{2} \mathbf{X}_{1,1} \cos^2 \theta + \mathbf{X}_{1,2} \cos \theta \sin \theta + \frac{1}{2} \mathbf{X}_{2,2} \sin^2 \theta \right) + O(\rho^3)$$

and

$$\begin{aligned} \mathbf{N}(\mathbf{t}) &= [\mathbf{X}_1 + \rho(\mathbf{X}_{1,1} \cos \theta + \mathbf{X}_{1,2} \sin \theta) + O(\rho^2)] \times [\mathbf{X}_2 + \rho(\mathbf{X}_{1,2} \cos \theta + \mathbf{X}_{2,2} \sin \theta) + O(\rho^2)] = \\ &= (\mathbf{X}_1 \times \mathbf{X}_2) + \rho((\mathbf{X}_1 \times \mathbf{X}_{1,2}) \cos \theta + (\mathbf{X}_1 \times \mathbf{X}_{2,2}) \sin \theta - (\mathbf{X}_2 \times \mathbf{X}_{1,1}) \cos \theta - (\mathbf{X}_2 \times \mathbf{X}_{1,2}) \sin \theta) + O(\rho^2) \end{aligned}$$

This implies that

$$(\mathbf{X}(\mathbf{t}) - \mathbf{X}(\mathbf{s})) \cdot (\mathbf{X}(\mathbf{t}) - \mathbf{X}(\mathbf{s})) = \rho^2 (E \cos^2 \theta + 2F \sin \theta \cos \theta + G \sin^2 \theta) + O(\rho^3)$$

and

$$(\mathbf{X}(\mathbf{t}) - \mathbf{X}(\mathbf{s})) \cdot \mathbf{N}(\mathbf{t}) = -\frac{1}{2} \rho^2 (L \cos^2 \theta + 2M \sin \theta \cos \theta + N \sin^2 \theta) + O(\rho^3)$$

Then the thesis immediately descends. Note that the limit in (7) is never infinite because its denominator can be written as $\mathbf{v}^T A \mathbf{v}$ with $\mathbf{v}^T = (\cos \theta, \sin \theta)$ and with A denoting the symmetric definite positive matrix $\begin{pmatrix} E & F \\ F & G \end{pmatrix}$ associated with the first fundamental form of \mathbf{X} . ■

Clearly, when the boundary conditions in (1) are of Dirichlet type, the unknown in (4) is the flux $\phi := (\partial u / \partial \mathbf{n})|_{\Gamma}$, belonging to $H^{-1/2}(\Gamma)$ and the CBIE becomes

$$\int_{\Gamma} \mathcal{G}_{\kappa}(\mathbf{x}, \mathbf{y}) \phi(\mathbf{y}) d\Gamma_{\mathbf{y}} = c(\mathbf{x}) u_{\text{D}}(\mathbf{x}) + \int_{\Gamma} \frac{\partial \mathcal{G}_{\kappa}}{\partial \mathbf{n}_{\mathbf{y}}}(\mathbf{x}, \mathbf{y}) u_{\text{D}}(\mathbf{y}) d\Gamma_{\mathbf{y}}, \quad \mathbf{x} \in \Gamma. \quad (8)$$

Note that this is an integral equation of the general type

$$V_{\kappa} \phi(\mathbf{x}) = f(\mathbf{x}), \quad \mathbf{x} \in \Gamma, \quad (9)$$

where f denotes a known function and where the single layer operator $V_{\kappa} : H^{-1/2}(\Gamma) \rightarrow H^{1/2}(\Gamma)$ is an elliptic isomorphism defined as,

$$V_{\kappa} \phi(\mathbf{x}) := \int_{\Gamma} \mathcal{G}_{\kappa}(\mathbf{x}, \mathbf{y}) \phi(\mathbf{y}) d\Gamma_{\mathbf{y}}.$$

Conversely, when Neumann conditions are dealt with, the unknown in (4) is the acoustic potential $\phi := u|_{\Gamma}$, with $\phi \in H^{1/2}(\Gamma)$ and the CBIE becomes

$$\int_{\Gamma} \frac{\partial \mathcal{G}_{\kappa}}{\partial \mathbf{n}_{\mathbf{y}}}(\mathbf{x}, \mathbf{y}) \phi(\mathbf{y}) d\Gamma_{\mathbf{y}} + c(\mathbf{x}) \phi(\mathbf{x}) = + \int_{\Gamma} \mathcal{G}_{\kappa}(\mathbf{x}, \mathbf{y}) u_{\text{N}}(\mathbf{y}) d\Gamma_{\mathbf{y}} \quad \mathbf{x} \in \Gamma. \quad (10)$$

This is an integral equation of the general type

$$(c(x)I + K_{\kappa})\phi(\mathbf{x}) = f(\mathbf{x}), \quad \mathbf{x} \in \Gamma, \quad (11)$$

associated with the operator $cI + K_{\kappa}$, where I denotes the identity operator and $K_{\kappa} : H^{1/2}(\Gamma) \rightarrow H^{1/2}(\Gamma)$ is the following double layer operator,

$$K_{\kappa} \phi(\mathbf{x}) := \int_{\Gamma} \frac{\partial \mathcal{G}_{\kappa}}{\partial \mathbf{n}_{\mathbf{y}}}(\mathbf{x}, \mathbf{y}) \phi(\mathbf{y}) d\Gamma_{\mathbf{y}}.$$

Note that in our case the right hand side f in both (9) and (11) is just the right hand side respectively of (8) and (10) and also that clearly it is in any case $\phi = \phi(\mathbf{x}, \kappa)$.

If ϕ is available, the solution $u = u(\mathbf{x}, \kappa)$, $\mathbf{x} \in \Omega^{[\ell]}$ of the BVP in (1) is obtained by using the so called *representation formula*,

$$u(\mathbf{x}, \kappa) = \pm \left(\int_{\Gamma} \mathcal{G}_{\kappa}(\mathbf{x}, \mathbf{y}) \frac{\partial u}{\partial \mathbf{n}}(\mathbf{y}) d\Gamma_{\mathbf{y}} - \int_{\Gamma} \frac{\partial \mathcal{G}_{\kappa}}{\partial \mathbf{n}_{\mathbf{y}}}(\mathbf{x}, \mathbf{y}) u(\mathbf{y}) d\Gamma_{\mathbf{y}} \right), \quad \mathbf{x} \in \Omega^{[\ell]}, \quad (12)$$

where the sign is positive if $\ell = i$ (interior problem) and negative otherwise. We note that the numerical implementation of this formula is not completely trivial because near singular integrals have to be approximated, when \mathbf{x} is very near to Γ . However, one can be merely interested in ϕ or in evaluating u just at points sufficiently far from Γ . For example, when an exterior problem is taken into account, often the interest is just in the *far field pattern* of u , that is into the recovery of u_{∞} , where

$$u_{\infty}(\mathbf{v}) := \lim_{r \rightarrow \infty} r e^{-ikr} u(r\mathbf{v}), \quad \mathbf{v} \in S^2,$$

where S^2 is a unit sphere in \mathbb{R}^3 centered in the origin. In such case we can rely in the following formula whose computation just requires rules for regular integrals,

$$u_{\infty}(\mathbf{v}) = \frac{1}{4\pi} \int_{\Gamma} \left(ik u(\mathbf{y}) (\mathbf{v} \cdot \mathbf{n}_{\mathbf{y}}) + \frac{\partial u}{\partial \mathbf{n}}(\mathbf{y}) \right) e^{-ik(\mathbf{v} \cdot \mathbf{y})} d\Gamma_{\mathbf{y}}.$$

3. Multi-patch Isogeometric model

In this section we introduce the IgA-BEM model, with respect to the geometry representation and the discretization space to express the numerical solution. The flexibility to model complex geometries in the 3D case is facilitated by adopting its multi-patch formulation. We assume that the boundary Γ is a union of M patches $\Gamma^{(\ell)}$, $\ell = 1, \dots, M$, and for $\ell \neq k$ it holds $\Gamma^{(\ell)} \cap \Gamma^{(k)} = \emptyset$ and $\partial\Gamma^{(\ell)} \cap \partial\Gamma^{(k)}$ is a boundary edge curve of each patch, a corner point of each patch or an empty set. To each patch $\Gamma^{(\ell)}$ we assign a geometry map $\mathbf{F}^{(\ell)}$, such that $\bar{\Gamma}^{(\ell)} = \text{Image}(\mathbf{F}^{(\ell)})$, $\mathbf{F}^{(\ell)} : [0, 1]^2 \rightarrow \bar{\Gamma}^{(\ell)} \subset \mathbf{R}^3$ is regular and belongs to $C^2([0, 1]^2)$.

Each \mathbf{F}_ℓ is written in the following standard NURBS form [13],

$$\mathbf{F}^{(\ell)}(\mathbf{t}) := \frac{\sum_{\mathbf{i} \in \mathcal{J}_g^{(\ell)}} w_{\mathbf{i}}^{(\ell)} \mathbf{Q}_{\mathbf{i}}^{(\ell)} \hat{B}_{\mathbf{i}, \mathbf{d}}^{(\ell)}(\mathbf{t})}{\sum_{\mathbf{i} \in \mathcal{J}_g^{(\ell)}} w_{\mathbf{i}}^{(\ell)} \hat{B}_{\mathbf{i}, \mathbf{d}}^{(\ell)}(\mathbf{t})}, \quad \mathbf{t} \in [0, 1]^2, \quad (13)$$

where a set $\{\mathbf{Q}_{\mathbf{i}}^{(\ell)} \in \mathbf{R}^3, \mathbf{i} \in \mathcal{J}_g^{(\ell)}\}$ defines a net of control points which, together with the associated set of positive weights $\{w_{\mathbf{i}}^{(\ell)} \in \mathbf{R}, \mathbf{i} \in \mathcal{J}_g^{(\ell)}\}$, is the basic element typically used in the CAD environment to design free-form surfaces. The tensor product B-spline basis function $\hat{B}_{\mathbf{i}, \mathbf{d}}^{(\ell)}(\mathbf{t}) := \hat{B}_{i_1, d_1}^{(\ell)}(t_1) \hat{B}_{i_2, d_2}^{(\ell)}(t_2)$, where $\mathbf{i} := (i_1, i_2) \in \mathcal{J}_g^{(\ell)}$, is of bi-degree $\mathbf{d} = (d_1, d_2)$, defined on $[0, 1]^2$ in variable $\mathbf{t} := (t_1, t_2)$ and with respect to the bidimensional knot array $T_g^{(\ell)}$ associated with the ℓ -th patch, $T_g^{(\ell)} := T_{g,1}^{(\ell)} \times T_{g,2}^{(\ell)}$, and $T_{g,1}^{(\ell)}$ and $T_{g,2}^{(\ell)}$ are both clamped knot vectors with entries in the interval $[0, 1]$. When two patches share an edge $C_{\ell,k} := \partial\Gamma^{(\ell)} \cap \partial\Gamma^{(k)}$ for $\ell \neq k$, the shared edge is a NURBS curve. For simplicity we usually assume it to be parametrized with the same geometry map for both patches, up to reversion in directions and direction swapping in the parametric space.

In order to define the finite dimensional space where the density function ψ is approximated in our IgA-BEM setting, let us first introduce the notation $T_j^{(\ell)}$ and $h_j^{(\ell)}$ to refer respectively to a (possible) refinement of $T_{g,j}^{(\ell)}$ and to the maximal distance between successive knots in $T_j^{(\ell)}$, $j = 1, 2$. Then, setting $h^{(\ell)} := \max\{h_1^{(\ell)}, h_2^{(\ell)}\}$ and introducing a set of bivariate indices $\mathcal{J}^{(\ell)}$ for the basis functions, we denote with $\hat{\mathcal{S}}_{h^{(\ell)}}^{(\ell)}$ the spline space generated by the tensor product B-spline basis $\{\hat{B}_{\mathbf{j}, \mathbf{d}}^{(\ell)} : \mathbf{j} = (j_1, j_2) \in \mathcal{J}^{(\ell)}\}$ of bi-degree \mathbf{d} defined on $[0, 1]^2$ with respect to the bidimensional knot array $T^{(\ell)} := T_1^{(\ell)} \times T_2^{(\ell)}$.

3.1. Discontinuous basis

When no continuity constraint is imposed across patches for the basis functions, the global space used to approximate the unknown density function ψ is

$$\mathcal{S}_{h, \mathbf{d}} := \text{span}\{B_{\mathbf{j}, \mathbf{d}}^{(\ell)} : \mathbf{j} \in \mathcal{J}^{(\ell)}, \ell = 1, \dots, M\},$$

where $h := \max\{h^{(\ell)}, \ell = 1, \dots, M\}$ and

$$B_{\mathbf{j}, \mathbf{d}}^{(\ell)}(\mathbf{x}) = \begin{cases} \hat{B}_{\mathbf{j}, \mathbf{d}}^{(\ell)} \circ \mathbf{F}^{(\ell)-1}(\mathbf{x}), & \text{if } \mathbf{x} \in \Gamma^{(\ell)}, \\ 0, & \text{otherwise.} \end{cases}$$

Clearly with this setting we have that the global number N_{DOF} of degrees of freedom used to approximate ψ is such that

$$N_{\text{DOF}} = \sum_{\ell=1}^M |\mathcal{J}^{(\ell)}|,$$

where $|\mathcal{J}^{(\ell)}|$ is the cardinality of the set. In this setting it is convenient to select $|\mathcal{J}^{(\ell)}|$ distinct collocation points belonging to the interior of each patch $\Gamma^{(\ell)}$, $\ell = 1, \dots, M$. In particular we fix $\mathbf{x}_{\mathbf{j}}^{(\ell)} = \mathbf{F}^{(\ell)}(\mathbf{s}_{\mathbf{j}})$, $\mathbf{j} \in \mathcal{J}^{(\ell)}$, where $\{\mathbf{s}_{\mathbf{j}}^{(\ell)} : \mathbf{j} \in \mathcal{J}^{(\ell)}\}$ denotes a set of points in $(0, 1)^2$, defined as the Cartesian product of two sets of abscissas, the so-called improved Greville abscissas associated with $T_1^{(\ell)}$ and $T_2^{(\ell)}$ [26]. Note that the improved Greville abscissas are Greville abscissas, whose first and last elements are slightly moved toward the interior of the parametric interval.

Remark 1. In order to get a more flexible model, it is not necessary that the degree \mathbf{d} referred to in the notation $\mathcal{S}_{h,\mathbf{d}}$ is exactly that used for the geometry representation given in (13), even if it is a quite common assumption. Similarly, it is sometimes convenient to set the knot array $\mathbf{T}^{(\ell)}$ not as a refinement of $\mathbf{T}_{\mathbf{g}}^{(\ell)}$ to obtain an additional flexibility of the spline space.

Thus, a discrete version of the given variational Dirichlet (8) or Neumann (10) problem is obtained by approximating ϕ in the finite dimensional composite space $\mathcal{S}_{h,\mathbf{d}}$. The applied collocation method leads to a linear system

$$A \boldsymbol{\alpha} = \boldsymbol{\beta}. \quad (14)$$

The unknown entries in the vector $\boldsymbol{\alpha}$ are the coefficients which allow us to define our approximation ϕ_h of ϕ in the space $\mathcal{S}_{h,\mathbf{d}}$ patch-wisely as follows,

$$\phi_h(\mathbf{x}) := \sum_{\ell=1}^M \sum_{\mathbf{j} \in \mathcal{J}^{(\ell)}} \alpha_{\mathbf{j}}^{(\ell)} B_{\mathbf{j},\mathbf{d}}^{(\ell)}(\mathbf{x}), \quad \mathbf{x} \in \Gamma.$$

The square system matrix $A \in \mathbb{C}^{N_{\text{DOF}} \times N_{\text{DOF}}}$ and the right-hand side vector $\boldsymbol{\beta} \in \mathbb{C}^{N_{\text{DOF}}}$ have a block representation, $A = (A^{(\ell,k)})$, $\boldsymbol{\beta} = (\boldsymbol{\beta}^{(\ell)})$, for $\ell, k = 1, \dots, M$, where $A^{(\ell,k)} \in \mathbb{C}^{|\mathcal{J}^{(\ell)}| \times |\mathcal{J}^{(k)}|}$ and $\boldsymbol{\beta}^{(\ell)} \in \mathbb{C}^{|\mathcal{J}^{(\ell)}|}$. For each patch the entries of the submatrices are ordered by using a lexicographical ordering of the elements in $\mathcal{J}^{(\ell)}$, namely we identify a single index i with \mathbf{i} and j with \mathbf{j} . After this simplification, the entries of the linear system for the Dirichlet problem in the parametric domain read

$$A_{i,j}^{(\ell,k)} := \int_{[0,1]^2} \mathcal{G}_{\kappa}(\mathbf{x}_{\mathbf{i}}^{(\ell)}, \mathbf{F}^{(k)}(\mathbf{t})) \hat{B}_{\mathbf{j},\mathbf{d}}^{(k)}(\mathbf{t}) J^{(k)}(\mathbf{t}) d\mathbf{t}, \quad i = 1, \dots, |\mathcal{J}^{(\ell)}|, \quad j = 1, \dots, |\mathcal{J}^{(k)}|, \quad (15)$$

$$\boldsymbol{\beta}_i^{(\ell)} := \sum_{k=1}^M \int_{[0,1]^2} \frac{\partial \mathcal{G}_{\kappa}}{\partial \mathbf{n}_y}(\mathbf{x}_{\mathbf{i}}^{(\ell)}, \mathbf{F}^{(k)}(\mathbf{t})) u_{\text{D}}(\mathbf{F}^{(k)}(\mathbf{t})) J^{(k)}(\mathbf{t}) d\mathbf{t} + \frac{1}{2} u_{\text{D}}(\mathbf{x}_{\mathbf{i}}^{(\ell)}), \quad i = 1, \dots, |\mathcal{J}^{(\ell)}|, \quad (16)$$

where $\hat{B}_{\mathbf{j},\mathbf{d}}^{(k)} \in \hat{\mathcal{S}}_{h^{(k)}}^{(k)}$ and $J^{(k)}$ represents the infinitesimal surface area element on the k -th patch,

$$J^{(k)}(\cdot) := \left\| \frac{\partial \mathbf{F}_k}{\partial t_1}(\cdot) \times \frac{\partial \mathbf{F}_k}{\partial t_2}(\cdot) \right\|_2.$$

Conversely, for the Neumann case we have

$$A_{i,j}^{(\ell,k)} := \int_{[0,1]^2} \frac{\partial \mathcal{G}_{\kappa}}{\partial \mathbf{n}_y}(\mathbf{x}_{\mathbf{i}}^{(\ell)}, \mathbf{F}^{(k)}(\mathbf{t})) \hat{B}_{\mathbf{j},\mathbf{d}}^{(k)}(\mathbf{t}) J^{(k)}(\mathbf{t}) d\mathbf{t} + \frac{1}{2} \hat{B}_{\mathbf{j},\mathbf{d}}^{(k)}(\mathbf{s}_{\mathbf{i}}^{(\ell)}), \quad i = 1, \dots, |\mathcal{J}^{(\ell)}|, \quad j = 1, \dots, |\mathcal{J}^{(k)}|, \quad (17)$$

$$\boldsymbol{\beta}_i^{(\ell)} := \sum_{k=1}^M \int_{[0,1]^2} \mathcal{G}_{\kappa}(\mathbf{x}_{\mathbf{i}}^{(\ell)}, \mathbf{F}^{(k)}(\mathbf{t})) u_{\text{N}}(\mathbf{F}^{(k)}(\mathbf{t})) J^{(k)}(\mathbf{t}) d\mathbf{t}, \quad i = 1, \dots, |\mathcal{J}^{(\ell)}|. \quad (18)$$

3.2. C^0 continuous basis

Let us denote the space of B-spline functions that join with C^0 regularity across patches by $\mathcal{S}_{h,\mathbf{d}}^0 := \mathcal{S}_{h,\mathbf{d}} \cap C^0(\Gamma)$. For simplicity let us assume that any two adjacent patches $\Gamma^{(\ell)}, \Gamma^{(k)}$ with a common boundary curve $\mathcal{C}_{\ell,k}$ have the same knot vector on the edges of the patches. Namely, on ℓ -th patch we consider the knot vector $T_1^{(\ell)}$ if $\mathbf{F}^{(\ell)}(t_1, 0)$ or $\mathbf{F}^{(\ell)}(t_1, 1)$ define the curve $\mathcal{C}_{\ell,k}$, and $T_2^{(\ell)}$ in the other case. The same procedure is done for k -th patch. Our assumption then states that the two vectors $T_i^{(\ell)}, T_j^{(k)}$ need to coincide (up to a possible reversion of one knot sequence, e.g., when $\mathbf{F}^{(\ell)}(1, t_2) = \mathbf{F}^{(k)}(1, 1 - t_2)$). For a more general setting to describe the geometry and the discretization space without the matching of adjacent knot vectors we refer to [7].

The so-called interior basis functions for $\mathcal{S}_{h,\mathbf{d}}^0$ includes all basis functions $B_{\mathbf{j},\mathbf{d}}^{(\ell)}$ from $\mathcal{S}_{h,\mathbf{d}}$, whose corresponding B-splines $\hat{B}_{\mathbf{j},\mathbf{d}}^{(\ell)}$ vanish on $\partial([0,1]^2)$. The so-called edge or vertex basis functions are obtained by identifying and summing together the remaining basis functions from $\mathcal{S}_{h,\mathbf{d}}$ with shared knot vectors. More precisely, an edge basis

function $B \in \mathcal{S}_{h,\mathbf{d}}^0$ associated to $C_{\ell,k}$ is a sum of two remaining (not interior) functions $B_{\mathbf{i},\mathbf{d}}^{(\ell)}$ and $B_{\mathbf{j},\mathbf{d}}^{(k)}$ from $\mathcal{S}_{h,\mathbf{d}}$, that vanish at the endpoints of $C_{\ell,k}$ and satisfy $\hat{B}_{\mathbf{i},\mathbf{d}}^{(\ell)} \circ \mathbf{F}^{(\ell)-1}(\mathbf{x}) = \hat{B}_{\mathbf{j},\mathbf{d}}^{(k)} \circ \mathbf{F}^{(k)-1}(\mathbf{x})$ for every $\mathbf{x} \in C_{\ell,k}$. Similarly, a vertex function associated to a patch corner vertex \mathbf{x}_v , is defined as a sum of all basis functions $B_{\mathbf{i},\mathbf{d}}^{(\ell)}$ from $\mathcal{S}_{h,\mathbf{d}}$, $\ell = 1, \dots, M$ and $\mathbf{i} \in \mathcal{J}^{(\ell)}$, that satisfy $\hat{B}_{\mathbf{i},\mathbf{d}}^{(\ell)} \circ \mathbf{F}^{(\ell)-1}(\mathbf{x}_v) \neq 0$.

In all our experiments with the C^0 continuous basis we have fixed the collocation points as a set of images of Cartesian products of standard Greville abscissas on $[0, 1]^2$, mapped to $\bar{\Gamma}^{(\ell)}$ via map $\mathbf{F}^{(\ell)}$ for all $\ell = 1, \dots, M$, and by counting just once the repeated points, which appear on the boundary curves of patches.

The approximate solution ϕ_h is constructed similarly to the discontinuous case, bearing in mind a variation in the collocation points and a sum of adequate entries in (15),(17) over all suitable k to evaluate integrals that span over the patches $\Gamma^{(k)}$ adjacent to the $\Gamma^{(\ell)}$.

4. Quadratures

4.1. Singularity extraction

Let us introduce our novel numerical integration method for integrals (15)–(18), which makes an efficient function–by–function assembly phase possible. For the sake of simplicity, we refer just to the one patch setting, i.e., we assume $M = 1$, thus avoiding any reference to the patch index. Some considerations about integration in the more general multi-patch setting are given at the end of the section.

It is convenient to write the two singular kernels \mathcal{G}_κ and $\partial\mathcal{G}_\kappa/\partial\mathbf{n}_y$ as in (5) and (6) and analyze, which terms are singular, hence a singular integration has to be considered, and which terms define regular integrals. As already noted in Section 2, the real part in (5) is weakly singular at $r = 0$ with its non-singular part $\cos(\kappa r)$ smooth under the assumption of a smooth geometry parameterization. For the same reason, its imaginary part is a smooth function. Similarly, the factor $\mathbf{r} \cdot \mathbf{n}_y/r^3$ of the real part in (6) is weakly singular, while the other factor, $(\cos(\kappa r) + \kappa \sin(\kappa r)r)$, is smooth. Finally, taking onto account Proposition 1, we know that the imaginary part in (6) is in general only C^1 continuous at $r = 0$ because the factor $\mathbf{r} \cdot \mathbf{n}_y/r^2$ is bounded and $(\sin(\kappa r)/r - \kappa \cos(\kappa r))$ has a double zero at $r = 0$.

Remark 2. *In our experiments it was enough to consider the splitting with C^1 continuous of the imaginary part in (6) to make the computations easier. If higher order of smoothness is needed, we can treat these integrals similarly as the singular ones, treating the part $\mathbf{r} \cdot \mathbf{n}_y/r^2$ as the “less regular part” of the integrand, while the remaining part $(\sin(\kappa r)/r - \kappa \cos(\kappa r))$ is an analytical function.*

In order to give a compact introduction of our quadrature approach, first we denote with $\mathbf{s} \in [0, 1]^2$ the pre-image of a fixed generic collocation point \mathbf{x} and then we refer to the following general form representing any of the singular integrals in (15)–(18)

$$\int_{R_j} U(\mathbf{s}, \mathbf{t}) \hat{B}_{\mathbf{j},\mathbf{d}}(\mathbf{t}) g(\mathbf{t}) d\mathbf{t}, \quad \mathbf{x} = \mathbf{F}(\mathbf{s}), \quad (19)$$

where $\hat{B}_{\mathbf{j},\mathbf{d}}$ is B-spline basis function, $R_j := \text{supp}\{\hat{B}_{\mathbf{j},\mathbf{d}}\}$, U refers to any of the following two weakly singular kernels of the singular and double layer potential,

$$U(\mathbf{s}, \mathbf{t}) := \frac{1}{\|\mathbf{F}(\mathbf{s}) - \mathbf{F}(\mathbf{t})\|_2} \quad \text{and} \quad U(\mathbf{s}, \mathbf{t}) := \frac{(\mathbf{F}(\mathbf{s}) - \mathbf{F}(\mathbf{t})) \cdot \mathbf{n}_t}{\|\mathbf{F}(\mathbf{s}) - \mathbf{F}(\mathbf{t})\|_2^3},$$

$\mathbf{n}_t := ((\partial\mathbf{F}/\partial t_1) \times (\partial\mathbf{F}/\partial t_2))(\mathbf{t})$ and g is a smooth given function.

Remark 3. *Integrals defining the entries of β do not include the basis functions $\hat{B}_{\mathbf{j},\mathbf{d}}$ directly. To split the integration domain $[0, 1]^2$ into smaller subdomains and arrive to the above general form, we introduce additional knot vectors, $T_{r,1}, T_{r,2}$, and inside (16) and (18) we add a sum of all B-spline basis functions $\hat{B}_{\mathbf{j},\mathbf{0}}$ of degree zero, defined on $T_{r,1} \times T_{r,2}$. Therefore, the approach to evaluate integrals in β is very similar to the one for the system matrix A .*

First of all we observe that the integral in (19) is effectively singular or nearly singular only if

$$\min_{\mathbf{t} \in R_j} \|\mathbf{x} - \mathbf{F}(\mathbf{t})\|_2 \leq \delta \quad (20)$$

for a given threshold $\delta \geq 0$. When the condition (20) is not satisfied, the kernel U is considered regular and integration rules for regular integrals are applied. Conversely, when the kernel U in (19) is weakly singular or even near singular, we preliminarily adopt a regularization technique based on the subtraction of singularity,

$$\int_{R_j} U(\mathbf{s}, \mathbf{t}) \hat{B}_{j,d}(\mathbf{t}) g(\mathbf{t}) d\mathbf{t} = \int_{R_j} (U(\mathbf{s}, \mathbf{t}) - U_s^m(\mathbf{s} - \mathbf{t})) \hat{B}_{j,d}(\mathbf{t}) g(\mathbf{t}) d\mathbf{t} + \int_{R_j} U_s^m(\mathbf{s} - \mathbf{t}) \hat{B}_{j,d}(\mathbf{t}) g(\mathbf{t}) d\mathbf{t}, \quad (21)$$

where U_s^m is an approximation of $U(\mathbf{s}, \bullet)$, obtained by truncating a particular series expansion of U about the singular point $\mathbf{t} = \mathbf{s}$ after the m -th term; see [12] for the first application of these expansions in the simplest form and [15] for detailed construction and analysis. Note that the singularity subtraction technique that splits an integral into two ones is applied only to a smaller portion of integrals. In this case, the first term of the right hand side of (21) becomes a *regularized integral* while the second one is a singular integral with a simplified singular kernel. The continuity of the integrand in the regularized integral is controlled by the number m of terms in U_s^m .

Remark 4. A regularization technique based on division step,

$$\int_{R_j} U(\mathbf{s}, \mathbf{t}) \hat{B}_{j,d}(\mathbf{t}) g(\mathbf{t}) d\mathbf{t} = \int_{R_j} \frac{U(\mathbf{s}, \mathbf{t})}{U_s^m(\mathbf{s} - \mathbf{t})} U_s^m(\mathbf{s} - \mathbf{t}) \hat{B}_{j,d}(\mathbf{t}) g(\mathbf{t}) d\mathbf{t} \quad (22)$$

is an elegant and effective tool to deal with singular integrals for 2D potential problems [5, 11]. Despite being considered in some recent publications for 3D potential problems [12, 10], we do not consider it in this study due to increased difficulty to properly approximate the singular kernel of the double layer potential. Owing to the division step, the regularized kernel becomes singular if U_s^m has roots inside the integration domain. For additional analysis of the latter regularization technique see [15].

The continuity of the integrand in the regularized integrals is equal to C^{m-2} at $\mathbf{t} = \mathbf{s}$ for the chosen $m \geq 1$ (with C^{-1} we denote functions that are integrable in the standard sense but have discontinuities of the first kind at $\mathbf{t} = \mathbf{s}$), if the geometry map \mathbf{F} is a smooth enough function [15]. By defining local coordinates $\mathbf{z} := \mathbf{s} - \mathbf{t}$, the kernel reads

$$U_s^m(\mathbf{z}) = \sum_{k=1}^m R_s(\mathbf{z})^{-2(k+\mu)+1} P_{s,3k+2\mu-3}^{[k]}(\mathbf{z}), \quad (23)$$

where $R_s(\mathbf{z}) := \sqrt{\mathbf{z}^T M_s \mathbf{z}}$ is a square root of a bivariate quadratic homogeneous polynomial and M_s corresponds to the first fundamental form of a smooth surface,

$$M_s = \begin{bmatrix} \left(\frac{\partial \mathbf{F}}{\partial t_1} \cdot \frac{\partial \mathbf{F}}{\partial t_1} \right) (\mathbf{s}) & \left(\frac{\partial \mathbf{F}}{\partial t_1} \cdot \frac{\partial \mathbf{F}}{\partial t_2} \right) (\mathbf{s}) \\ \left(\frac{\partial \mathbf{F}}{\partial t_2} \cdot \frac{\partial \mathbf{F}}{\partial t_1} \right) (\mathbf{s}) & \left(\frac{\partial \mathbf{F}}{\partial t_2} \cdot \frac{\partial \mathbf{F}}{\partial t_2} \right) (\mathbf{s}) \end{bmatrix},$$

$P_{s,3k+2\mu-3}^{[k]}$ are suitable homogenous polynomials of degrees $3k + 2\mu - 3$, and $\mu = 0$ and $\mu = 1$ for \mathcal{G}_κ and $\partial \mathcal{G}_\kappa / \partial \mathbf{n}_y$, respectively. Note that coefficients inside R_s and $P_{s,3k+2\mu-3}^{[k]}$ depend on a chosen \mathbf{s} and on derivatives of map \mathbf{F} . For example, for $m = 1$ the kernel of the single layer potential is approximated with

$$U_s^1(\mathbf{z}) = \frac{1}{4\pi} [R_s(\mathbf{z})^{-1}],$$

while the kernel in the double layer potential is approximated by

$$U_s^1(\mathbf{z}) = \frac{1}{4\pi} [R_s(\mathbf{z})^{-3} P_{s,2}^{[1]}(\mathbf{z})],$$

where

$$\begin{aligned}
P_{s,2}^{[1]}(\mathbf{z}) &= d_{2,0}z_1^2 + d_{1,1}z_1z_2 + d_{0,2}z_2^2, \\
d_{2,0} &= \frac{1}{2} \left(-\frac{\partial^2 F_3}{\partial t_1^2} \frac{\partial F_2}{\partial t_1} \frac{\partial F_1}{\partial t_2} + \frac{\partial^2 F_2}{\partial t_1^2} \frac{\partial F_3}{\partial t_1} \frac{\partial F_1}{\partial t_2} + \frac{\partial^2 F_3}{\partial t_1^2} \frac{\partial F_1}{\partial t_1} \frac{\partial F_2}{\partial t_2} - \frac{\partial^2 F_1}{\partial t_1^2} \frac{\partial F_3}{\partial t_1} \frac{\partial F_2}{\partial t_2} - \frac{\partial^2 F_2}{\partial t_1^2} \frac{\partial F_1}{\partial t_1} \frac{\partial F_3}{\partial t_2} + \frac{\partial^2 F_1}{\partial t_1^2} \frac{\partial F_2}{\partial t_1} \frac{\partial F_3}{\partial t_2} \right) (\mathbf{s}), \\
d_{1,1} &= \left(-\frac{\partial^2 F_3}{\partial t_1 \partial t_2} \frac{\partial F_2}{\partial t_1} \frac{\partial F_1}{\partial t_2} + \frac{\partial^2 F_2}{\partial t_1 \partial t_2} \frac{\partial F_3}{\partial t_1} \frac{\partial F_1}{\partial t_2} + \frac{\partial^2 F_3}{\partial t_1 \partial t_2} \frac{\partial F_1}{\partial t_1} \frac{\partial F_2}{\partial t_2} - \frac{\partial^2 F_1}{\partial t_1 \partial t_2} \frac{\partial F_3}{\partial t_1} \frac{\partial F_2}{\partial t_2} - \frac{\partial^2 F_2}{\partial t_1 \partial t_2} \frac{\partial F_1}{\partial t_1} \frac{\partial F_3}{\partial t_2} + \frac{\partial^2 F_1}{\partial t_1 \partial t_2} \frac{\partial F_2}{\partial t_1} \frac{\partial F_3}{\partial t_2} \right) (\mathbf{s}), \\
d_{0,2} &= \frac{1}{2} \left(\frac{\partial F_3}{\partial t_1} \frac{\partial^2 F_2}{\partial t_2^2} \frac{\partial F_1}{\partial t_2} - \frac{\partial F_2}{\partial t_1} \frac{\partial^2 F_3}{\partial t_2^2} \frac{\partial F_1}{\partial t_2} - \frac{\partial F_3}{\partial t_1} \frac{\partial^2 F_1}{\partial t_2^2} \frac{\partial F_2}{\partial t_2} + \frac{\partial F_1}{\partial t_1} \frac{\partial^2 F_3}{\partial t_2^2} \frac{\partial F_2}{\partial t_2} + \frac{\partial F_2}{\partial t_1} \frac{\partial^2 F_1}{\partial t_2^2} \frac{\partial F_3}{\partial t_2} - \frac{\partial F_1}{\partial t_1} \frac{\partial^2 F_2}{\partial t_2^2} \frac{\partial F_3}{\partial t_2} \right) (\mathbf{s}).
\end{aligned}$$

Relating to the more general multi-patch setting, when source point $\mathbf{x} = \mathbf{F}^{(\ell)}(\mathbf{s})$ and integration variable $\mathbf{y} = \mathbf{F}^{(k)}(\mathbf{t})$ belong to different adjacent patches, $\Gamma^{(\ell)}$ and $\Gamma^{(k)}$, the integral in (19) is nearly singular if condition (20) is satisfied, and regular otherwise. In the latter case, the procedure is similar to the one for regular integrals on one patch. In the first case, when the integral is considered near singular but $k \neq \ell$, we construct again the approximate kernel U_s^m , as in (23), that is a truncated series expansion of $U(\mathbf{s}, \bullet)$ about the source point \mathbf{s} and let \mathbf{z} be a local variable for U_s^m .

Numerical integration across patches poses an additional challenge. Since the parameterization of the geometry is prescribed patch-wisely, the series expansion U_s^m is limited to $\Gamma^{(\ell)}$. To get a suitable extrapolation of U_s^m across the ℓ -th patch to the k -th patch, we need to construct a local reparameterization of the integration domain $\mathbf{F}^{(k)-1}(\bar{\Gamma}^{(k)})$ with respect to the reference domain $\mathbf{F}^{(\ell)-1}(\bar{\Gamma}^{(\ell)}) = [0, 1]^2$. The local reparameterization of the integration domain is constructed by applying a suitable linear transformation $\mathbf{W} : [0, 1]^2 \rightarrow \mathbb{R}^2$, consisting of rotations and translations of $[0, 1]^2$, to match a boundary or a vertex of the reference domain $[0, 1]^2$; see Figure 1, where the origin of a patch is indicated by the accompanying two arrows. That way the definition of the expansion U_s^m is directly expanded to the neighbouring patch and at each $\mathbf{y} \in \Gamma^{(k)}$ the value of the expansion is equal to $U_s^m(\mathbf{s} - \mathbf{W}(\mathbf{t}))$. In our tests we observe that also extrapolated values of U_s^m to $\Gamma^{(k)}$ give sufficiently accurate values of U for 3- and 4-patch smooth contacts that appear in the parametrizations of the considered spherical and toroidal geometries.

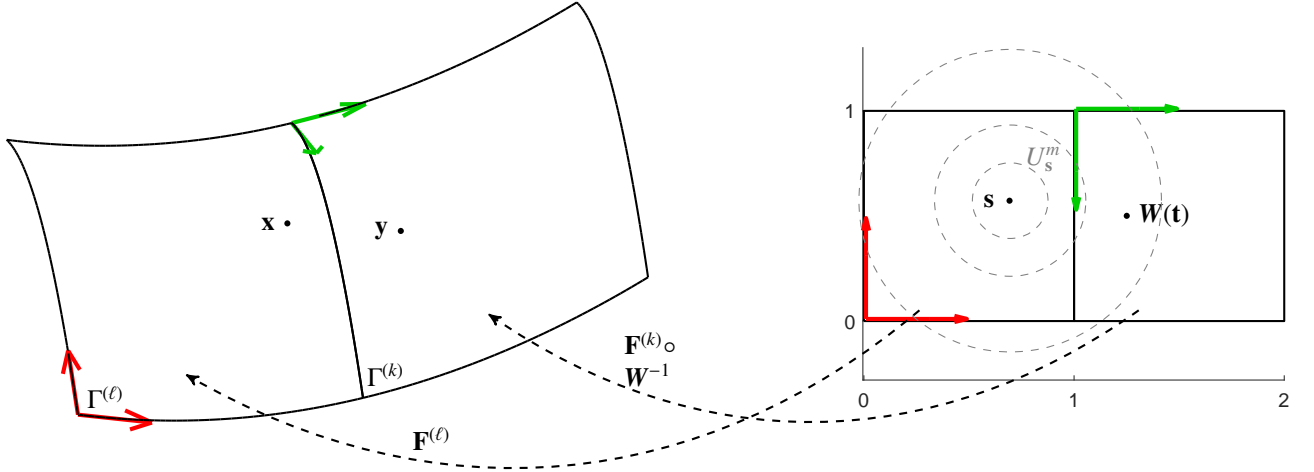


Figure 1: Constructing a local domain for two adjacent patches.

For example, a function $\mathbf{t} \mapsto |U(\mathbf{s}, \mathbf{t}) - U_s^2(\mathbf{s} - \mathbf{t})|$, which is the absolute value of the regularized part of the integrand in (21) for kernel of the single layer potential, is depicted in Figure 2. The figure shows the regularized function in the parametric domain on 4 adjacent patches, related to a section of toroidal geometry (see the beginning of Section 5). Since the extrapolation of U_s^2 to the 3 adjacent patches gives sufficiently bounded values and oscillations

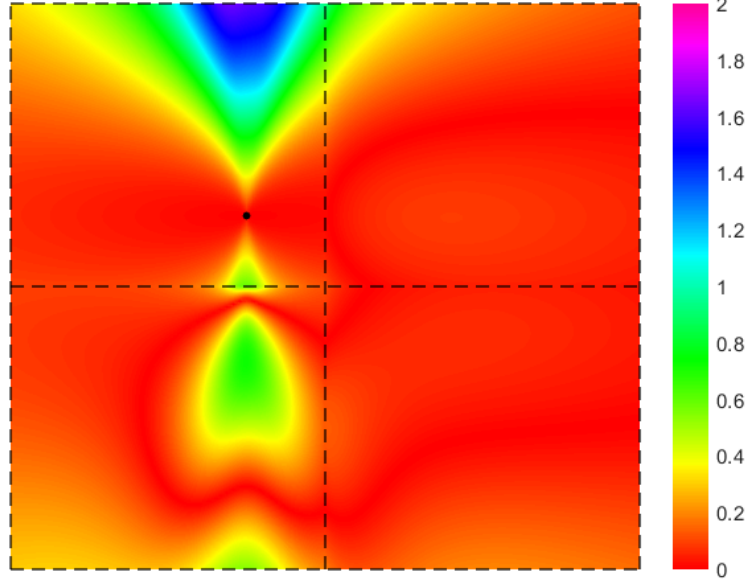


Figure 2: The absolute value of the regularized function on the 4-patch configuration, corresponding to a section of torus. In the top left corner the source point s (represented as a black dot) and the integration point belong to the same patch, whereas on to the three adjacent patches the values of U_s^2 are obtained by an extrapolation.

of the regularized function, it can be effectively treated in the numerical scheme for regular integrals, presented in Section 4.3.

4.2. B-spline quasi-interpolation scheme

To approximate integrals in 3D collocation BEM, we utilise the 2D Quasi Interpolation (QI) scheme firstly introduced in [4]. With such approach a bivariate function f is approximated on a rectangle R by using a QI spline tensor product operator $f \rightarrow \sigma_f := \sum_{\mathbf{i} \in \mathcal{J}_R} \lambda_{\mathbf{i}} \hat{B}_{\mathbf{i}, \mathbf{p}}$, where $\{\hat{B}_{\mathbf{i}, \mathbf{p}}, \mathbf{i} \in \mathcal{J}_R\}$ is the tensor-product B-spline basis generating the chosen finite dimensional space of splines defined in R and \mathcal{J}_R is a local a set of bivariate indices associated to the local basis on R . The scheme is the tensor-product extension of the univariate Hermite QI scheme introduced in [17]. Hence each coefficient $\lambda_{\mathbf{i}}, \mathbf{i} \in \mathcal{J}_R$ is computed as a linear combination of the values in a suitable local subset of spline knots by f , by both its first partial derivatives and also by its second mixed derivative, see [4] for details. However, in the present work we rely on a derivative-free Lagrange variant of such QI scheme, since we are interested to employ it for quadrature. Such variant is obtained approximating the required derivative values by suitable finite difference formulas. Then, collecting with lexicographical order all the coefficients $\lambda_{\mathbf{i}}, \mathbf{i} \in \mathcal{J}_R$ in a vector Λ , in compact matrix notation we have

$$\Lambda = (\hat{C}^{(p)})^T \mathbf{f}, \quad (24)$$

where \mathbf{f} is a vector collecting with the same ordering all the values of f at the knots of the spline space and

$$\hat{C}^{(p)} := \left((\hat{A}_2^T \otimes \hat{A}_1^T) - (\hat{A}_2^T \otimes (\hat{B}_1^T D_{i_1})) - ((\hat{B}_2^T D_{i_2}) \otimes \hat{A}_1^T) + ((\hat{B}_2^T D_{i_2}) \otimes (\hat{B}_1^T D_{i_1})) \right)^T. \quad (25)$$

In the above formula \hat{A}_i, \hat{B}_i denote the two banded matrices explicitly reported, for example, in [5] which are associated to the univariate original Hermite scheme formulated in the i -th direction, $i = 1, 2$; $D_i, i = 1, 2$ are the matrices associated with the two analogous directional finite difference formulas used by the considered QI variant of the original scheme for approximating the first partial derivatives.

4.3. B-spline quadrature rules for regular integrals

Since in the assayed BIEs the regular integrands consist of the product between a bivariate regular function f with a tensor product B-spline $\hat{B}_{\mathbf{j},\mathbf{d}}$, we need to construct a quadrature rule to evaluate numerically the following integral:

$$\int_{R_{\mathbf{j}}} f(\mathbf{t})\hat{B}_{\mathbf{j},\mathbf{d}}(\mathbf{t}) d\mathbf{t}.$$

The first step consists in approximating f with the QI scheme previously described. In this way we can write:

$$f \approx \sigma_f = \sum_{\mathbf{i} \in \mathcal{J}_{R_{\mathbf{j}}}} \lambda_{\mathbf{i}} \hat{B}_{\mathbf{i},\mathbf{p}},$$

where $\hat{B}_{\mathbf{i},\mathbf{p}}$ denotes a tensor product B-spline of bi-degree $\mathbf{p} = (p_1, p_2)$ which is an element of a basis generating a local spline space defined in $R_{\mathbf{j}}$. Hence

$$\int_{R_{\mathbf{j}}} f(\mathbf{t})\hat{B}_{\mathbf{j},\mathbf{d}}(\mathbf{t}) d\mathbf{t} \approx \int_{R_{\mathbf{j}}} \sigma_f(\mathbf{t})\hat{B}_{\mathbf{j},\mathbf{d}}(\mathbf{t}) d\mathbf{t}. \quad (26)$$

The product $\sigma_f \hat{B}_{\mathbf{j},\mathbf{d}}$ is a new spline that can be expressed in term of another B-spline basis defined in a suitable local “product” spline space of bi-degree $\mathbf{p} + \mathbf{d}$. Generalizing the idea developed in [19, 11] for the one-dimensional case, the coefficients of $\sigma_f \hat{B}_{\mathbf{j},\mathbf{d}}$ in the B-spline basis of the product space can be written as $G_{\mathbf{j}}^{\top} \mathbf{\Lambda}$, with $\mathbf{\Lambda}$ defined by QI as specified in (24). In the current bivariate setting the matrix $G_{\mathbf{j}}$ is defined as $G_{\mathbf{j}} := G_{j_1}^{(p_1, d_1)} \otimes G_{j_2}^{(p_2, d_2)}$, where $G_{j_1}^{(p_1, d_1)}$ and $G_{j_2}^{(p_2, d_2)}$ are suitable direction-wise coefficient matrices and $\mathbf{j} = (j_1, j_2)$. The dimension of $G_{\mathbf{j}}$ is $|\mathcal{J}_{R_{\mathbf{j}}}| \times N_{\pi_{\mathbf{j}}}$, where $N_{\pi_{\mathbf{j}}}$ denotes the dimension of the introduced local product spline space. Thus, the integral in (26) can finally be evaluated as,

$$\int_{R_{\mathbf{j}}} f(\mathbf{t})\hat{B}_{\mathbf{j},\mathbf{d}}(\mathbf{t}) d\mathbf{t} \approx \mathbf{v}^{\top} G_{\mathbf{j}}^{\top} \mathbf{\Lambda} = \mathbf{v}^{\top} G_{\mathbf{j}}^{\top} (\hat{C}^{(p)})^{\top} \mathbf{f},$$

where the matrix $\hat{C}^{(p)}$ is defined in (25) and \mathbf{v} denotes a vector of suitable length collecting in lexicographical order the following integrals of each B-spline $\hat{B}_{\mathbf{k},\mathbf{p}+\mathbf{d}}$ of the basis of the local product spline space,

$$\int_{R_{\pi}} \hat{B}_{\mathbf{k},\mathbf{p}+\mathbf{d}}(\mathbf{t}) d\mathbf{t} = \frac{|\text{supp}(\hat{B}_{\mathbf{k},\mathbf{p}+\mathbf{d}})|}{(p_1 + d_1 + 1)(p_2 + d_2 + 1)}, \quad \mathbf{k} \in \mathcal{J}_{\pi_{\mathbf{j}}},$$

where $\mathcal{J}_{\pi_{\mathbf{j}}}$ is a set of $N_{\pi_{\mathbf{j}}}$ distinct multi-indices, as usually done to identify a tensor-product B-spline basis. In the case of regularized integrals, for each collocation point \mathbf{s} , this approach is applied to the function $f_{\mathbf{s}}(\mathbf{t}) := (U(\mathbf{s}, \mathbf{t}) - U_{\mathbf{s}}^m(\mathbf{s} - \mathbf{t}))g(\mathbf{t})$, as outlined in formula (21).

4.4. B-spline quadrature rules for singular integrals

Let us focus now on the rules developed for the numerical approximation of the second addend on the right of (21) which involves the simplified singular kernel $U_{\mathbf{s}}^m(\mathbf{s} - \mathbf{t})$. The first step is analogous to that adopted for regular integrals, since g is approximated with σ_g by using the same QI approach and then multiplied by $\hat{B}_{\mathbf{j},\mathbf{d}}$. Thus we can write

$$\int_{R_{\mathbf{j}}} U_{\mathbf{s}}^m(\mathbf{s} - \mathbf{t})\hat{B}_{\mathbf{j},\mathbf{d}}(\mathbf{t})g(\mathbf{t}) d\mathbf{t} \approx \mathbf{v}^{\top} G_{\mathbf{j}}^{\top} (\hat{C}^{(p)})^{\top} \mathbf{g},$$

where \mathbf{g} is the vector whose entries are the values of g used by the QI operator but now \mathbf{v} collects in suitable order all the following integrals

$$\int_{R_{\mathbf{j}}} U_{\mathbf{s}}^m(\mathbf{s} - \mathbf{t})\hat{B}_{\mathbf{k},\mathbf{p}+\mathbf{d}}(\mathbf{t}) d\mathbf{t}, \quad \mathbf{k} \in \mathcal{J}_{\pi_{\mathbf{j}}}.$$

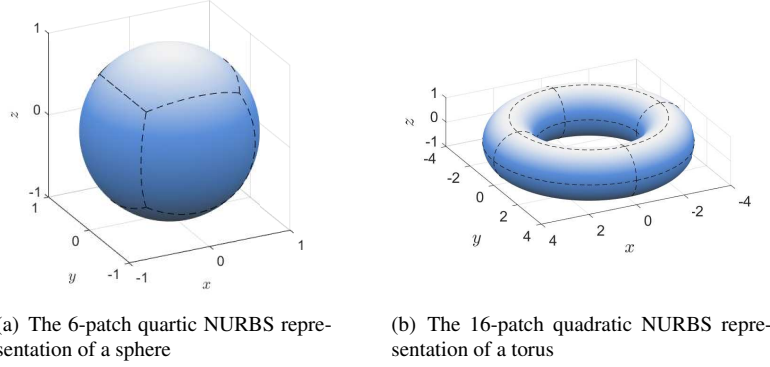


Figure 3: The two NURBS multipatch representations of a sphere and a torus.

Thus, in order to complete the definition of the quadrature rule, we are interested in deriving the exact expression of the above integrals. For this aim we introduce the following notation,

$$I_{r_1, r_2}^{q_1, q_2}(k_1, k_2) := \int_{\tau_{k_1}^{(1)}}^{\tau_{k_1+r_1+1}^{(1)}} \int_{\tau_{k_2}^{(2)}}^{\tau_{k_2+r_2+1}^{(2)}} U_{\mathbf{s}}^m(\mathbf{s} - \mathbf{t})(t_1 - s_1)^{q_1}(t_2 - s_2)^{q_2} \hat{B}_{k_1, r_1}(t_1) \hat{B}_{k_2, r_2}(t_2) dt_1 dt_2,$$

where $\mathbf{k} = (k_1, k_2)$ and $\tau_{k_\ell+j}^{(\ell)}$, $j = 0, \dots, r_\ell$, $\ell = 1, 2$ define the two univariate knot vectors active in the definition of $\hat{B}_{\mathbf{k}, \mathbf{p}+\mathbf{d}}$, where for brevity we have set $r_\ell := p_\ell + d_\ell$ which is the univariate degree in the ℓ -th direction of the product space. Then, using the tensor product extension of the Cox-de Boor recurrence relation for B-splines [8], we can express $I_{r_1, r_2}^{q_1, q_2}(k_1, k_2)$ as a linear combination of $I_{r_1-1, r_2-1}^{q_1+m_1, q_2+m_2}(k_1+w_1, k_2+w_2)$, where $m_1, m_2, w_1, w_2 = 0, 1$. Starting with $q_1 = q_2 = 0$ and iterating this recurrence up to involve just B-splines of degree 0 in both coordinate directions, the procedure can be completed, provided that the following *basic moments* have been preliminarily computed for q_ℓ and i_ℓ respectively ranging in the set of indices $0, \dots, p_\ell + r_\ell$ and $k_\ell, \dots, k_\ell + r_\ell$, $\ell = 1, 2$,

$$I_{0,0}^{q_1, q_2}(i_1, i_2) = \int_{\tau_{i_1}^{(1)}}^{\tau_{i_1+1}^{(1)}} \int_{\tau_{i_2}^{(2)}}^{\tau_{i_2+1}^{(2)}} U_{\mathbf{s}}^m(\mathbf{s} - \mathbf{t})(t_1 - s_1)^{q_1}(t_2 - s_2)^{q_2} dt_1 dt_2 = \int_{s_1 - \tau_{i_1}^{(1)}}^{s_1 - \tau_{i_1+1}^{(1)}} \int_{s_2 - \tau_{i_2}^{(2)}}^{s_2 - \tau_{i_2+1}^{(2)}} U_{\mathbf{s}}^m(\mathbf{z})(-z_1)^{q_1}(-z_2)^{q_2} dz_1 dz_2.$$

For this aim we have been relying on the analytical expressions derived in [15] and computed with a help of Wolfram Mathematica software.

5. Numerical examples

In this section we test our model to numerically solve one interior and two exterior Helmholtz problems, all with Neumann boundary conditions, which are more commonly considered for applications.

The two well-known benchmarks for exterior problems are the pulsating sphere and the rigid scattering on a sphere; see for instance [25, 23, 21]. The sphere has radius $R = 1$ and it is parameterized by 6 quartic NURBS patches, see Figure 3(a) and refer to [6] for details. As in [9], the considered quartic NURBS parameterization based on cube topology is the preferred choice to the 8-patch tiling in order to avoid singularities in the geometry description.

The last example is a standard acoustic problem interior to a torus; see for example [25, 23]. The toroidal surface Γ has inner and outer radii respectively equal to 1 and 3 and is exactly represented in a 16-patch quadratic NURBS form, see Figure 3(b) and refer to [10] for details.

For the discretization space V , on each patch we employ standard tensor product B-splines of different bi-degrees $d_1 = d_2$ and of highest continuity; in the last two experiments we enforce C^0 continuity for the basis functions across patch interfaces. The threshold distance parameter to switch between singular and regular integration rules is fixed to $\delta = 0.1$ for all experiments. The quality of the numerical results is always evaluated by considering the behavior of the error in terms of total degrees of freedom (N_{DOF}) or in terms of the number n of elements used for discretization

on each patch and in each coordinate direction. The reported error is the on-surface relative error measured in the $L^2(\Gamma)$ norm,

$$e_{L^2} = \frac{\|u_h - u^{ex}\|_{L^2(\Gamma)}}{\|u^{ex}\|_{L^2(\Gamma)}}.$$

5.1. Pulsating sphere

The following problem serves as a benchmark test for the developed quadrature rules; it is also referred to as a patch test for IgA-BEM. The model can be used for example to numerically compute the sound pressure at a distance r from the center of the sphere for a constant speed of wave in the radial direction. For the Neumann boundary conditions set to $u_N \equiv e^{i\kappa}(i\kappa - 1)/(4\pi)$ for $\mathbf{x} \in \Gamma$, the analytical solution is given as $u = e^{i\kappa r}/(4\pi r)$, hence the missing Cauchy data is $\phi \equiv e^{i\kappa}/(4\pi)$ for $\mathbf{x} \in \Gamma$.

Since the geometry representation of the sphere is exact and ϕ is constant over the entire boundary, the truncation error can be attributed solely to numerical integration. On each patch the knot vectors describing the local part of the discretization space $\hat{\mathcal{S}}_{h^{(\ell)}}^{(\ell)}$ are

$$T_{g,1}^{(\ell)} = T_{g,2}^{(\ell)} = \begin{bmatrix} 0 & 0.25 & 0.5 & 0.75 & 1 \end{bmatrix}.$$

We fix $\kappa = 1$ and $\mathbf{d} = (0, 0)$, and measure the L^2 error of the approximate solution with respect to different number of quadrature nodes on the support of B-splines. The number n_q of quadrature nodes increases in each coordinate direction with $n_q = 12\alpha + 1$, for $\alpha = 1, 2, \dots, 10$. The same quadrature nodes are used for singular, regularized and regular integrals.

In Figure 4(a) we observe that the error distribution (modulus of the difference between the exact and approximate solution) for $\alpha = 1, m = 2$ (number of terms in the singularity extraction), $p = 2$ (spline degree of the QI operator) is well evenly spread on the boundary with a slight increase of error at patch corners. In Figure 4(b) we can observe that error convergence order is impacted by the choice of m and p , since the integrand functions are C^0 and C^1 continuous for $m = 2$ and $m = 3$, respectively. For $m, p = 2$ the obtained order of convergence is 3. If we increase both m and p to 3, the order of convergence increases to 4.

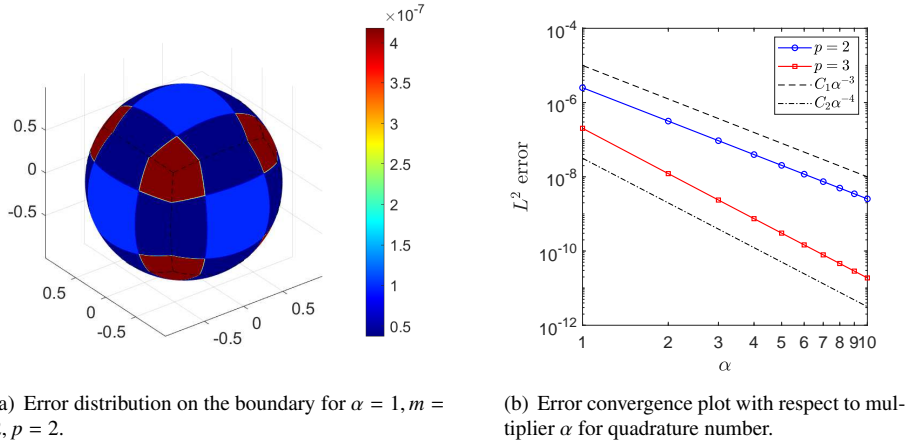


Figure 4: Pulsating sphere for $\kappa = 1$.

5.2. Rigid Scattering on a sphere

In rigid scattering (exterior) problems reformulated in the frequency domain, it is assumed that an acoustic pressure p_{inc} of amplitude A is produced by a wave vector $\kappa\mathbf{v}$, with \mathbf{v} denoting a unit vector prescribing the direction of the wave,

$$p_{inc}(\mathbf{x}) := Ae^{i\kappa(\mathbf{v}\cdot\mathbf{x})}.$$

Such pressure is incident on a rigid body represented by a volume $\Omega^{(i)}$ with boundary Γ , where the rigidity assumption implies that it reacts producing in $\Omega^{(e)}$ an additional scattered pressure field p verifying the Helmholtz equation in $\Omega^{(e)}$, the Sommerfield radiation condition at infinity and having a variation in the normal direction on Γ opposite to that of p_{inc} , see for example [25]. The scattered pressure p is the unknown to be determined in $\Omega^{(e)}$ and it can be written as the difference between a total pressure field p_{tot} and p_{inc} , where p_{tot} is such that

$$\begin{cases} p_{tot}(\mathbf{x}) &= p_{inc}(\mathbf{x}) + (V_\kappa \partial_n p_{tot}) - (K_\kappa p_{tot})(\mathbf{x}), \quad \mathbf{x} \in \Omega^{(e)} \\ \partial_n p_{tot}(\mathbf{x}) &= 0, \quad \forall \mathbf{x} \in \Gamma. \end{cases}$$

Note that in this experiment we assume Γ as a sphere with radius $R = 1$ (again parameterized as previously described) and so, for symmetry, without loss of generality we can assume $\mathbf{v} = (1, 0, 0)$. The problem can be used as a benchmark because the analytic expression of p is a priori known, see for example [21],

$$p(\mathbf{x}) = -A \sum_{n=0}^{\infty} \frac{i^n (2n+1) j_n'(\kappa R)}{h_n'(\kappa R)} P_n(\cos(\theta)) h_n(\kappa r),$$

where in our experiments we set $A = 1$ and n ranges from 1 to 10 because this is sufficient to study the convergence of our numerical scheme for the used frequencies. In this formula, assuming the sphere centered in \mathbf{O} , $r = \|\mathbf{x} - \mathbf{O}\|_2$, θ is the angle between the vector $\mathbf{x} - \mathbf{O}$ and \mathbf{v} , h_n and j_n are the spherical Hankel and Bessel functions of order n (the derivative with respect to its argument is denoted by $'$) and P_n is the Legendre polynomial of order n .

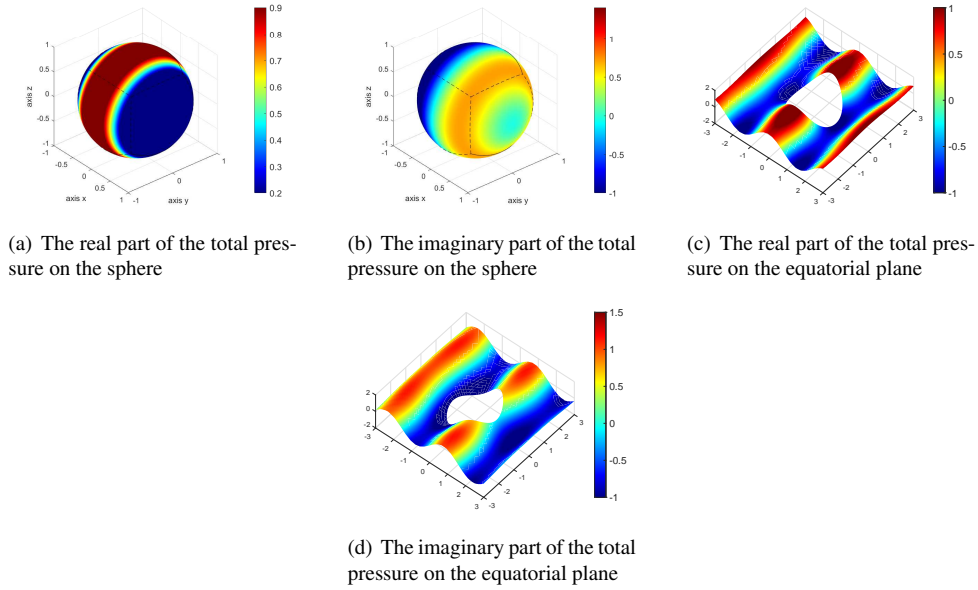


Figure 5: Rigid scattering on a sphere with $\kappa = 2$: on and off surface total pressure distributions.

The values considered for κ in the experiments are $\kappa = 1, 2, 3$ which in the air corresponds to a frequency of about 50, 100, 150 Hz. In the implementation we aim to approximate the unknown Dirichlet Cauchy datum $\phi = p_{tot}|_\Gamma$ (alternatively also denoted below just with u which denotes also its extension to $\Omega^{(e)}$). Thus, considering that the corresponding given Neumann datum is homogeneous, the boundary integral equation to be considered simplifies to the following one,

$$(K_\kappa + \frac{1}{2}I)\phi(\mathbf{x}) = p_{inc}(\mathbf{x}), \quad \mathbf{x} \in \Gamma. \quad (27)$$

The discretization of this BIE has been done by using a globally C^0 multi-patch IgA space with the same size of uniform elements on each patch. For this experiment we consider the following simplification

$$\frac{\mathbf{r} \cdot \mathbf{n}}{r^2} = -\frac{1}{2R},$$

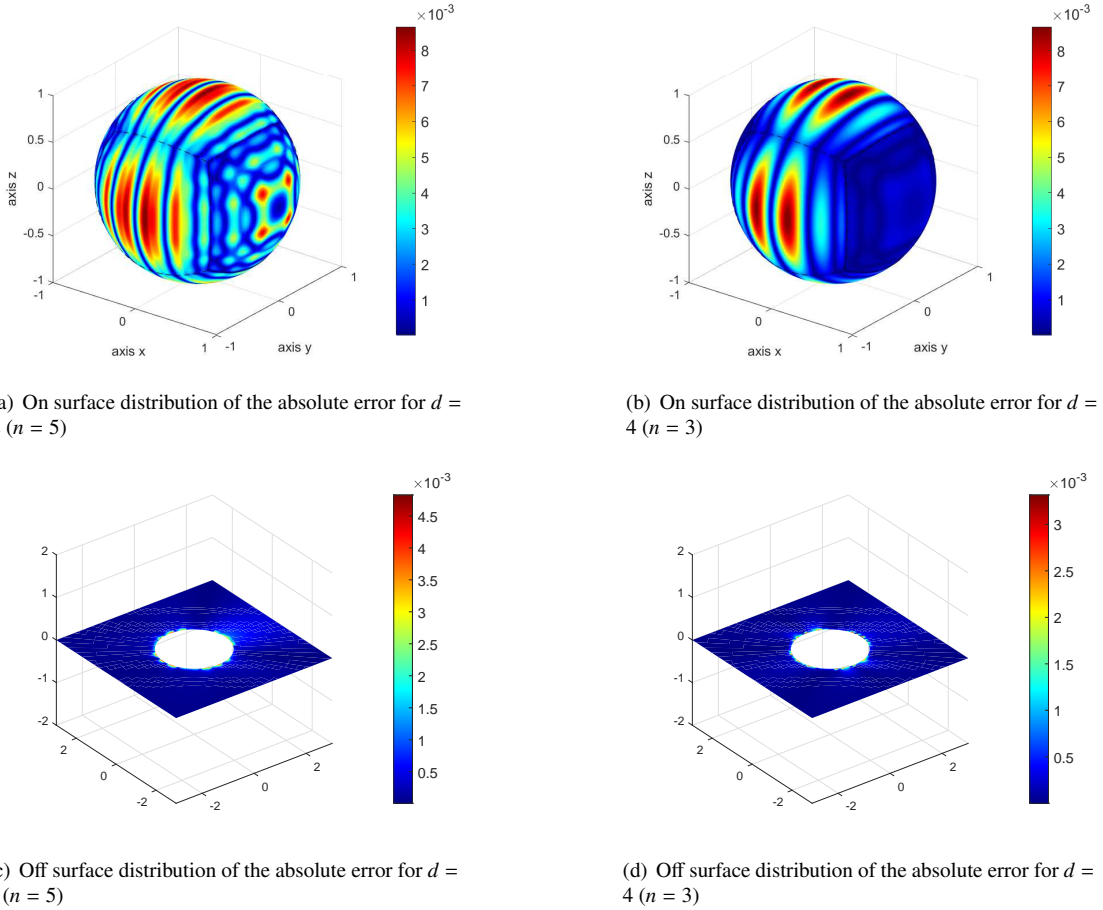
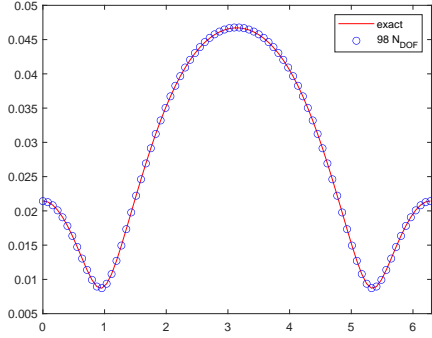


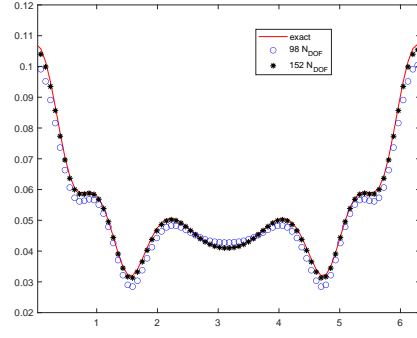
Figure 6: Rigid scattering on a sphere with $\kappa = 2$: on and off surface distribution of the absolute error ($N_{DOF} = 218$).

where \mathbf{n} points toward the center of the sphere since the considered problems are exterior. Then by taking into account (6) we use regular rules when the imaginary part of the double layer kernel K_κ is considered. Conversely, the rules for the weakly singular kernel $\mathbf{r} \cdot \mathbf{n}_y / r^3$ have been used with $m = 2$, when its real part is dealt with. In all the tests reported for this experiment for all the three kinds of quadrature rules the QI degree is 2 for the singular and regularized rules and it is 4 for the regular ones. Furthermore, the chosen number of QI nodes uniformly distributed in the support of each test B-spline function ($N_{w1} = N_{w2} = N_{r1} = N_{r2} = 7, 9, 16$, $N_1 = N_2 = 13, 17, 21$, respectively when $d := d_1 = d_2 = 2, 3, 4$) ensures that the number of quadrature nodes on each element is small for all the considered rules and not depending on d .

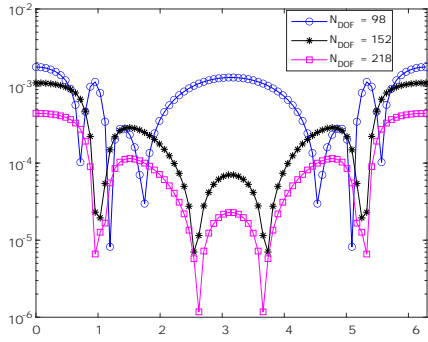
In order to underline the oscillating nature of the solution of (27) and of the related domain solution, Figure 5 shows the real and the imaginary part of the exact Cauchy datum $\phi = p_{tot}|_\Gamma$ for $\kappa = 2$, together with the corresponding real and imaginary parts of the total pressure in an area of the equatorial plane exterior to the sphere. The upper and lower parts of Figure 6 show the distribution of the absolute error obtained with both the choices $d = 2$ and $d = 4$, respectively on the sphere and on the equatorial plane. Note that the number of degrees of freedom ($N_{DOF} = 218$) is the same on the left and on the right of this figure, since the number n^2 of elements in each patch is chosen in order to ensure the fulfillment of such goal, that is $n = 5$ for $d = 2$ and $n = 3$ for $d = 4$. This means that when $d = 4$,



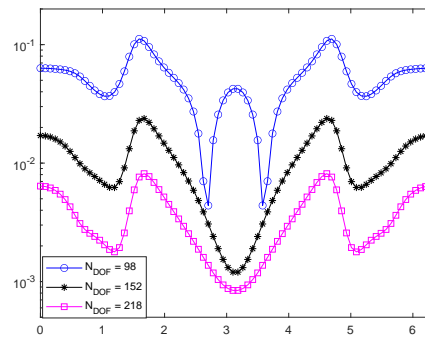
(a) Modulus of the exact and of the numerical solution on C for $\kappa = 1$.



(b) Modulus of the exact and of the numerical solution on C for $\kappa = 3$.



(c) Distribution of the error e_p on C for $\kappa = 1$.



(d) Distribution of the error e_p on C for $\kappa = 3$.

Figure 7: Rigid scattering on a sphere: results on the exterior equatorial circumference C ($d = 2, p = 2, 2, 4$).

the elements are larger than in the other case and so an analogous maximal error on the surface is acceptable. Note also that the error distribution on the sphere implies a slightly lower $L^2(\Gamma)$ relative error on surface for $d = 4$ (it is $3.20e - 03$ for $d = 2$ and $2.43e - 03$ for $d = 4$).

The off surface quality of our approach is further clarified by the plots reported in Figure 7. Focusing on the approximation of the modulus of the solution, the figure shows the results obtained on the exterior equatorial circumference C with radius 10 setting $d = 2$ (the other parameters are chosen as already described), as also done in [23], where the reported error is the following one

$$e_p(\mathbf{x}) := \frac{||u_h(\mathbf{x})| - |u^{ex}(\mathbf{x})||}{|u^{ex}(\mathbf{x})|}. \quad (28)$$

The figure outlines a good conformability between the moduli of the exact and of the numerical solution obtained with very few degrees of freedom for both $\kappa = 1$ and $\kappa = 3$. The quality of our exterior reconstructions can be further checked looking at the distribution on C of the error e_p .

In order to complete the analysis of the results for this experiment, we present also Figure 8, which shows the dependency from n of the $L^2(\Gamma)$ relative error for d ranging between 2 and 4, confirming its nice convergence behavior for all the considered values of κ .

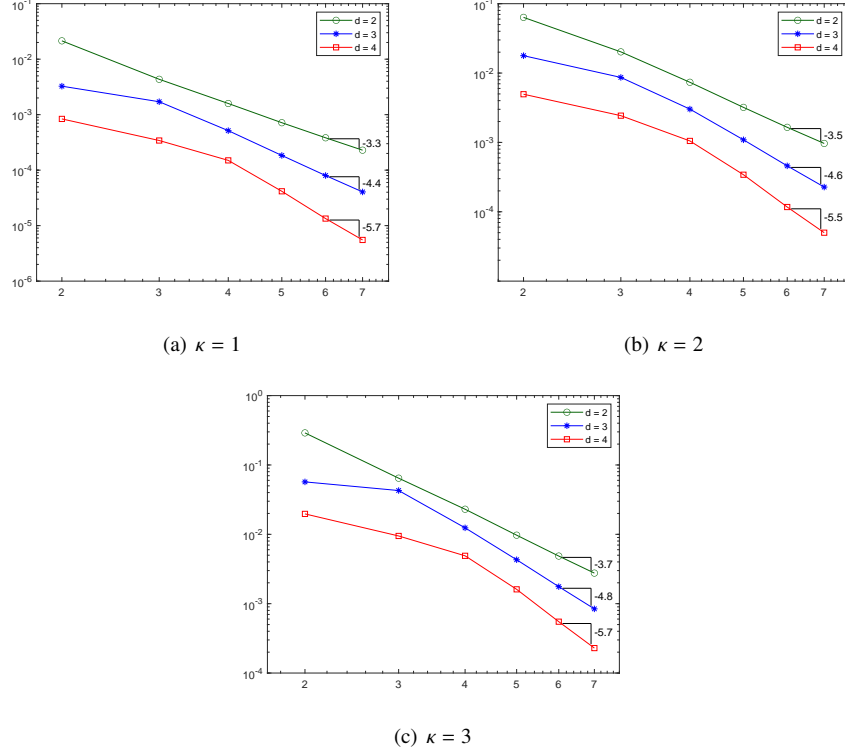


Figure 8: Rigid scattering on a sphere: behavior of the $L^2(\Gamma)$ error versus the number n of elements in each coordinate direction for each patch.

5.3. Acoustic problem interior to a torus

This last example is taken from [23]. The Helmholtz equation is considered with exact acoustic potential chosen to be

$$\phi(\mathbf{x}) = \sin(\kappa x / \sqrt{3}) \sin(\kappa y / \sqrt{3}) \sin(\kappa z / \sqrt{3}). \quad (29)$$

The Neumann datum is prescribed by computing the acoustic velocity field as $(\partial\phi/\partial\mathbf{n})(\mathbf{x})$ for $\mathbf{x} \in \Gamma$, where \mathbf{n} denotes the outward unit normal vector to the surface. In the experiments we considered the wavenumber $\kappa = 2$, and $d := d_1 = d_2 = 2, 3$ using a global C^0 discretization space. Regarding the adopted quadrature scheme, we use QI degree 2 for regularized and singular kernels (with $m = 2$) while QI degree 4 is employed for regular integrands. The number of quadrature points have been set to 7 for singular and regular integrals and to 13 for the regularised integrands when $d = 2$. In the case $d = 3$ we used 9 quadrature nodes for singular and regularised integrals; for regular integrals we used 13 nodes. In every case, the quadrature nodes are uniformly distributed, per parametric direction, on the support of each B-spline basis function.

While the imaginary part of the acoustic potential ϕ is zero on the entire boundary Γ , the chosen wavenumber produces several oscillation in the real part of ϕ , see Figure 9 (a). As we can see from Figure 9 (b) the error e_{L^2} is plotted with respect to h and the convergence rate equal to $d + 1$ can be observed. In Figure 9 (c) and (d) the absolute error for the real part and the imaginary part of the unknown acoustic potential ϕ is shown, respectively.

6. Conclusion

In this paper we address 3D Helmholtz problems using isogeometric BEMs and relying on conformal multi-patch smooth geometries and spline discretization spaces. The governing boundary integral equations are numerically approximated by a collocation scheme. The introduced quadrature rules for both regular and singular integrals are

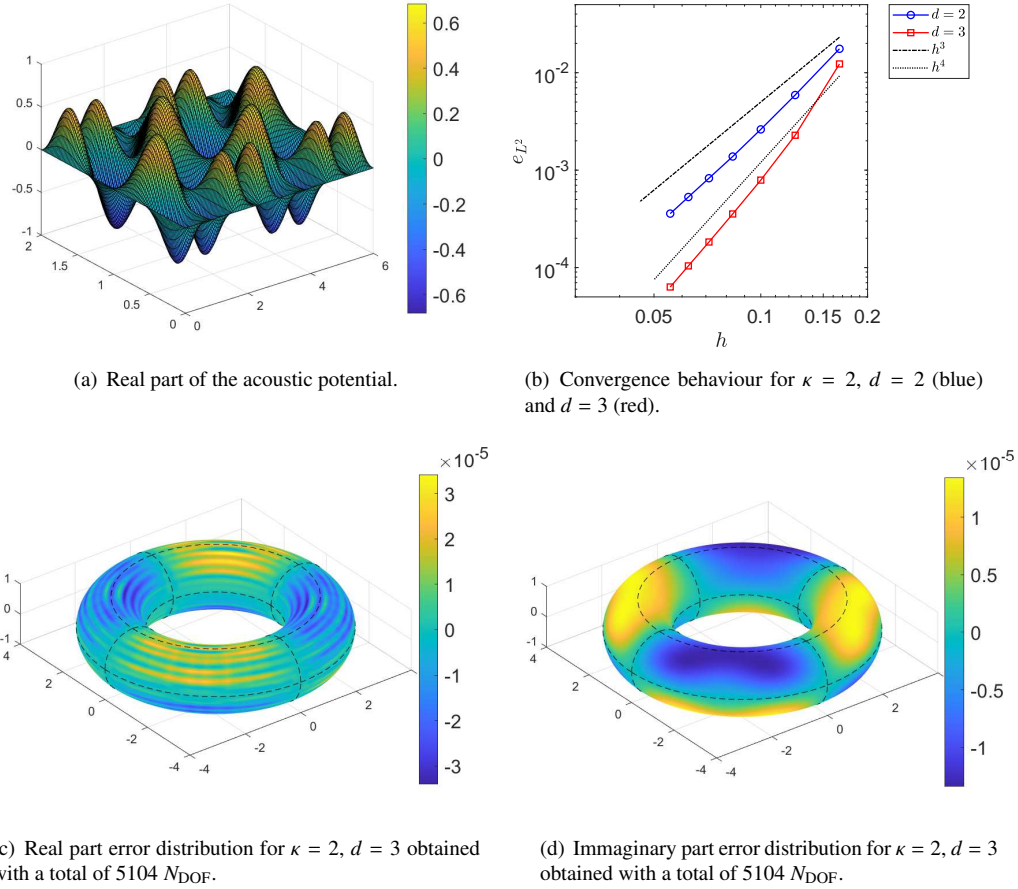


Figure 9: Acoustic problem interior to a torus.

tailored for B-splines and they allow a profitable function-by-function matrix assembly. Numerical results confirm the effectiveness of the method by achieving sufficient accuracy of the numerical solution with a small number of evenly distributed quadrature nodes.

A possible interesting future work includes a generalization of the proposed simulation model to non-conformal discretization spaces and parameterization. Since the employed singularity extraction relies on the analytical extension of smooth kernels in the parametric space, an approach that can handle more general types of contacts between patches in the conformal and non-conformal setting would improve the accuracy of the method.

Acknowledgements

Tadej Kanduč was partially funded for developing this research by SIMAI-ACRI, which is gratefully acknowledged. The research of Antonella Falini was founded by PON Project AIM 1852414 CUP H95G18000120006 ATT1. The Italian authors are members of the INdAM Research group GNCS. The INdAM support through GNCS and Finanziamenti Premiali SUNRISE is gratefully acknowledged.

References

- [1] Aimi, A., Diligenti, M., Sampoli, M., Sestini, A., 2016. Isogeometric Analysis and Symmetric Galerkin BEM: a 2D numerical study. *Appl Math Comp* 272, 173–186.

- [2] Atkinson, K., 1997. The numerical solution of integral equations of the second kind. Cambridge Monographs on Applied and Computational Mathematics. Cambridge University Press, New York.
- [3] Beer, G., Marussig, B., Duenser, C., 2020. The Isogeometric Boundary Element Method. Springer.
- [4] Bracco, C., Giannelli, C., Mazzia, F., Sestini, A., 2016. Bivariate hierarchical hermite spline quasi-interpolation. *BIT Numer Math* 56 (4), 1165–1188.
- [5] Calabrò, F., Falini, A., Sampoli, M., Sestini, A., 2018. Efficient quadrature rules based in spline quasi-interpolation for application to IgA-BEMs. *J Comput Appl Math* 338, 153–167.
- [6] Cobb, J., 1988. Tiling the sphere with rational Bézier patches. Technical report UUCS-88-009, Computer Science, University of Utah.
- [7] Cottrell, J., Hughes, T., Bazilevs, Y., 2009. Isogeometric analysis: toward integration of CAD and FEA. John Wiley & Sons.
- [8] de Boor, C., 2001. A practical guide to splines, revised Edition. Vol. 27 of Applied Mathematical Sciences. Springer-Verlag, New York.
- [9] Dölz, J., Harbrecht, H., Kurz, S., Schöps, S., Wolf, F., 2018. A fast isogeometric bem for the three dimensional laplace-and helmholtz problems. *Comput Methods Appl Mech Engrg* 330, 83–101.
- [10] Falini, A., Giannelli, C., Kanduč, T., Sampoli, M., Sestini, A., 2022, in press, preprint at arXiv:2204.02607. A collocation IGA-BEM for 3D potential problems on unbounded domains. In: Manni, C., Speleers, H. (Eds.), Springer INdAM volume 'Geometric Challenges in Isogeometric Analysis'. Vol. 49 of Springer INdAM Series. Springer.
- [11] Falini, A., Giannelli, C., Kanduč, T., Sampoli, M. L., Sestini, A., 2019. An adaptive iga-bem with hierarchical b-splines based on quasi-interpolation quadrature schemes. *Int J Numer Methods Eng* 117 (10), 1038–1058.
- [12] Falini, A., Kanduč, T., Sampoli, M., Sestini, A., 2021. Cubature rules based on bivariate spline quasi-interpolation for weakly singular integrals. In: Fasshauer, G., Neamtu, M., Schumaker, L. (Eds.), Approximation Theory XVI: Nashville 2019. Springer, pp. 73–86.
- [13] Farin, G., Hosheek, J., Kim, M. S., 2002. Handbook of Computer Aided Geometric Design. Elsevier, Amsterdam.
- [14] Grebenkov, D., Nguyen, D., 2013. Geometrical structure of laplacian eigenfunctions. *SIAM Review* 55 (4), 601–667.
- [15] Kanduč, T., 2021. Isoparametric singularity extraction technique for 3D potential problems in BEM. submitted, preprint at arXiv:2203.11538.
- [16] Kirkup, S., 2019. The boundary element method in acoustics: a survey. *Appl Sci* 9, 1642.
- [17] Mazzia, F., Sestini, A., 2009. The BS class of Hermite spline quasi-interpolants on nonuniform knot distributions. *BIT* 49 (3), 611–628.
- [18] Mazzia, F., Sestini, A., 2012. Quadrature formulas descending from BS Hermite spline quasi-interpolation. *J Comput Appl Math* 236, 4105–4118.
- [19] Mørken, K., 1991. Some identities for products and degree raising of splines. *Contr Approx* 7, 195–208.
- [20] Schumaker, L., 2007. Spline functions: basic theory. Cambridge University Press.
- [21] Shaaban, A., Anitescu, C., Atroshchenko, E., Rabczuk, T., 2021. 3d isogeometric boundary element analysis and structural shape optimization for helmholtz acoustic scattering problems. *Comput Methods Appl Mech Engrg* 384, 113950.
- [22] Simpson, R., Bordas, S., Trevelyan, J., Rabczuk, T., 2012. A two-dimensional isogeometric boundary element method for elastostatic analysis. *Comput Methods Appl Mech Engrg* 209–212, 87–100.
- [23] Simpson, R., Scott, M., Taus, M., Thomas, D., Lian, H., 2014. Acoustic isogeometric boundary element analysis. *Comput Methods Appl Mech Engrg* 269, 265–290.
- [24] Venas, J., Jenserud, T., 2019. Exact 3d scattering solutions for spherical symmetric scatterers. *J. of Sound and Vibration* 440, 439–479.
- [25] Venas, J., Kvamsdal, T., 2020. Isogeometric boundary element method for acoustic scattering by a submarine. *Comput. Methods Appl. Mech. Engrg.* 359, 112670.
- [26] Wang, Y. J., Benson, D. J., 2015. Multi-patch nonsingular isogeometric boundary element analysis in 3D. *Comput. Methods Appl. Mech. Engrg.* 293, 71–91.